

## Synthesis of enhanced fluorescent graphene quantum dots for catecholamine neurotransmitter sensing

Thi Hoa Le\*, Dal Ho Lee\*\*, Ji Hyeon Kim\*, and Sang Joon Park\*,†

\*Department of Chemical and Biological Engineering, Gachon University, Seongnam 13120, Korea

\*\*Department of Electronics Engineering, Gachon University, Seongnam 13120, Korea

(Received 12 October 2019 • accepted 6 February 2020)

**Abstract**—We employed polypyrrole/graphene quantum dot (PPy/GQD) composites as a sensor for the simple and selective detection of catecholamine neurotransmitters (CNs), such as dopamine (DA), epinephrine (EP), norepinephrine (NE), which play vital roles in the peripheral and central nervous systems. The PPy/GQD composites showed strong fluorescence emission, which was significantly increased, by as much as greater than three times, compared to that of the pristine GQDs. In neutral solution, the CNs on the surface of the PPy/GQD composites were converted into a quinone structure, which triggered the fluorescence quenching of the PPy/GQD composites via a photo-induced electron transfer process. The CN concentration could be effectively monitored based on the quenching of the fluorescence signal of the PPy/GQDs. The quenching effect of DA is the fastest and most effective, followed by those of EP and NE, respectively, and the quenched fluorescence intensity of the PPy/GQDs was proportional to the concentration of DA (0.007–250 µM), EP (0.7–250 µM), and NE (5–500 µM). The present system was used for the quantification of CNs in human serum samples with acceptable results.

**Keywords:** Catecholamine Neurotransmitters, Quinone Structure, Fluorescence Quenching, Polypyrrole, Graphene Quantum Dots

### INTRODUCTION

Neurotransmitters are chemical messengers that play vital roles in transferring signals from one neuron to another neuron or other tissues [1]. Catecholamine neurotransmitters (CNs), which contain amino and catechol moieties in structure, are one of the most important classes of biological amine neurotransmitters, including dopamine (DA), norepinephrine (NE), and epinephrine (EP) [2]. Deficiency of CNs leads to many nervous diseases such as Huntington's chorea, Parkinson's and Alzheimer's diseases, Schizophrenia as well as depression and various cancerous tumors [3–5]. Therefore, the development of an effective method of CN detection is crucial. Recently, different methods have become available for CN determination, such as capillary electrophoresis (CE) [6], high performance liquid chromatography (HPLC) [7], electrochemistry [8], native fluorescence [9] and flow injection analysis [10]. These methods show good efficiency for determining CNs, but it is necessary to use expensive instruments and have complex procedures of preparing [11]. In addition, understanding of neurotransmitter metabolism and clarifying their function requires new experimental technique and enhanced analytical tools [1]. As far as fluorescence methods are concerned, they have some drawbacks: they require quite high amount of target substances to get detectable fluorescence responses, so LOD of this method is not as low as that of the others. In addition, in some cases, a searching of suitable complementary

strand that can bind tightly substance is necessary [1,12]. However, currently fluorescence-based methods are attracting significant interest because they not only overcome some of the weak points of existing techniques but also are simple, rapid, highly sensitive, non-polluting, and non-destructive [13,14].

Recently, graphene quantum dots (GQDs), which contain the outstanding characteristics of graphene and quantum dots, have been shown to have excellent potential for chemical and biological applications. GQDs consist of one or few layers of graphene fragments and smaller than 10 nm in size [15]. GQDs possess some distinct properties, such as good biocompatibility, chemical stability, low toxicity, easy water solubility, stable photoluminescence, and high electrical conductivity [16,17].

Over the years, many attempts have been made to combine carbon nanomaterials such as graphene, carbon nanofibers, carbon nanotubes and conducting polymers to produce functional composite materials having superior properties for applying in fundamental and technological perspectives [18,19]. Among a variety of polymers, polypyrrole (PPy) is a growing and promising class, mainly due to their extraordinary electrical, optical, thermal and non-toxic properties [20,21]. Based on these advantages, this material has potential applications in many areas, especially in sensing [22,23].

In this research, we present a sensitive and simple fluorescence sensor for CN detection by utilizing PPy/GQD composites. GQDs are attached on PPy sphere surfaces. The amine groups belonging to the PPy molecules probably enhance the fluorescence intensity of the GQDs via surface passivation [24,25], which creates suitable conditions for CN detection. In particular, in neutral solutions containing PPy/GQDs, CNs can be oxidized to form catecholamine-

\*To whom correspondence should be addressed.

E-mail: psj@gachon.ac.kr

Copyright by The Korean Institute of Chemical Engineers.

quinone structures which act as absorbers receiving electrons from PPy/GQDs, and later “turn off” the fluorescence of the PPy/GQDs. Therefore, the concentration of CNs can be determined from quenching fluorescence signals of PPy/GQDs.

## EXPERIMENTAL DETAILS

### 1. Materials

Phosphate buffer saline (PBS) ( $\text{pH}=7.4$ ),  $\text{FeCl}_2$ ,  $\text{H}_2\text{O}_2$ ,  $\text{NaOH}$ , pyrrole, citric acid monohydrate, dopamine, epinephrine, norepinephrine, tryptophan, GABA, aspartic acid, uric acid, succinic acid, glucose, lactose, sucrose, alanine, glycine, lysine, stearic acid, palmitic acid were obtained from Sigma-Aldrich and used without further purification. Deionized water was applied for all processes.

### 2. Instrument and Measurements

Transmission electron microscopy (TEM) was conducted using TEM (FEI, Tecnai, F30S-Twin). The photoluminescence (PL) and UV-Vis spectra were obtained using a G1103A UV-Vis spectrophotometer from Agilent, USA and a QuantaMaster TM 50 PTI spectrofluorometer from Photon Technology International, USA. Zeta potential measurements were by electrophoretic light scattering (Photolab Otsuka Electronics, ELS 8000). Fourier transform infrared (FTIR) spectroscopy measurements were carried out using a Nicolet 6700 spectrometer from Thermo Scientific.

### 3. Synthesis of PPy Microspheres

PPy microspheres were synthesized following the previous method [26]. First, 5 mL  $\text{H}_2\text{O}_2$  was added to a mixture of pyrrole (1 mL),  $\text{FeCl}_2$  (0.1 g), and  $\text{H}_2\text{O}$  (94 mL), which was allowed to react for 6 h. Subsequently, the sample was centrifuged to concentrate the products, and then byproducts and unreacted reactants were removed by washing with water. The as-synthesized PPy microspheres were diffused in water to obtain typical concentration.

### 4. Synthesis of GQDs and PPy/GQD Composites

First, 2 g of citric acid (CA) monohydrate was put into a 5-mL beaker and heated to 200 °C in an oven. After 30 min, the CA melted, yielding a pale yellow and, subsequently, orange liquid. The resulting liquid was dropped into mixture of 100 mL  $\text{NaOH}$  (10 mg/mL) and 200  $\mu\text{L}$  of a PPy dispersion (2.25 mg/mL) with vigorous stirring for 3 h. GQDs was prepared similarly to approach mentioned above without adding PPy dispersion. Finally, the obtained GQDs and PPy/GQDs were dialyzed in a dialysis bag (MCWO: 1,000 Da) for 72 h to obtain pure materials.

### 5. CN Detection

For CN detection, different amounts of each CN (DA, EP, and NE) were added to a series of solutions containing 500  $\mu\text{L}$  PPy/GQDs and 2,500  $\mu\text{L}$  PBS buffer ( $\text{pH}=7.4$ ). Next, the solution was diluted to the mark by using deionized water, then incubated at 25 °C for 3 h. The fluorescence spectra were measured from 400 to 600 nm under excitation at 370 nm.

### 6. Detection of Real Samples

In these experiments, 100  $\mu\text{L}$  human serum was added to a 3 mL solution of PPy/GQDs and PBS buffer ( $\text{pH}=7.4$ ) (v/v: 1 : 5). A quantity of the CN was added, followed by adding an amount of deionized water to the mark before fluorescence analysis without pretreatment. The different CNs in the human serum samples were detected by the method described above.

## 7. Selectivity Investigation

To confirm the selectivity of the fluorescence method, the effects of carbohydrates, amino acids, and common molecules on the PPy/GQD system were studied.

## RESULTS AND DISCUSSION

### 1. Characterization of the Composites

The GQDs and PPy/GQD composites were synthesized according to the method presented above. Fluorescence and UV-vis absorption spectroscopy were used to characterize optical properties of the composite (Fig. 1). As seen in Fig. 1, the spectrum of PPy contains no absorption peak, whereas the UV-vis maximum absorption of the GQDs and PPy/GQD composites is around 360 nm, which is the same as the value previously reported [26,27].

As shown in Fig. 2, the maximum fluorescence emission peaks of the GQDs and PPy/GQDs are at 458 nm when the excitation wavelength is 370 nm. Although there are no changes in the location of the emission peaks, the fluorescence intensity of the PPy/GQD composite is higher than that of the GQDs.

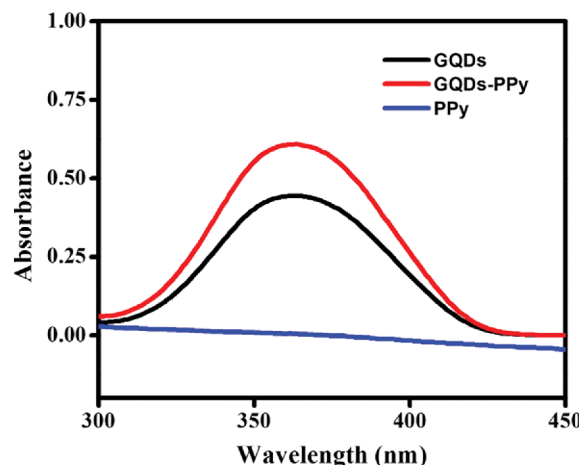


Fig. 1. UV-vis absorption spectra of PPy, GQDs, and PPy/GQDs.

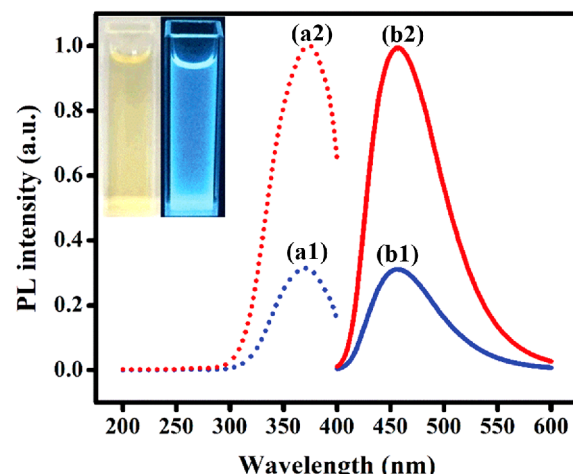
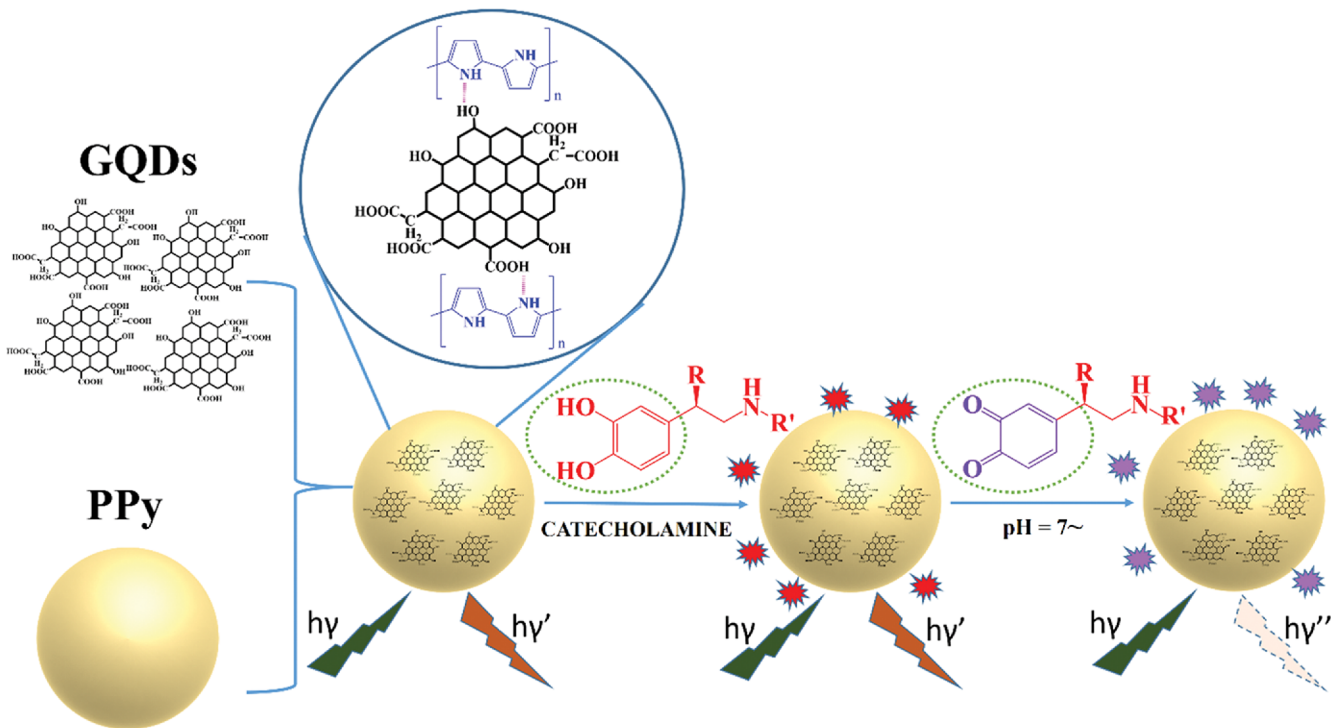
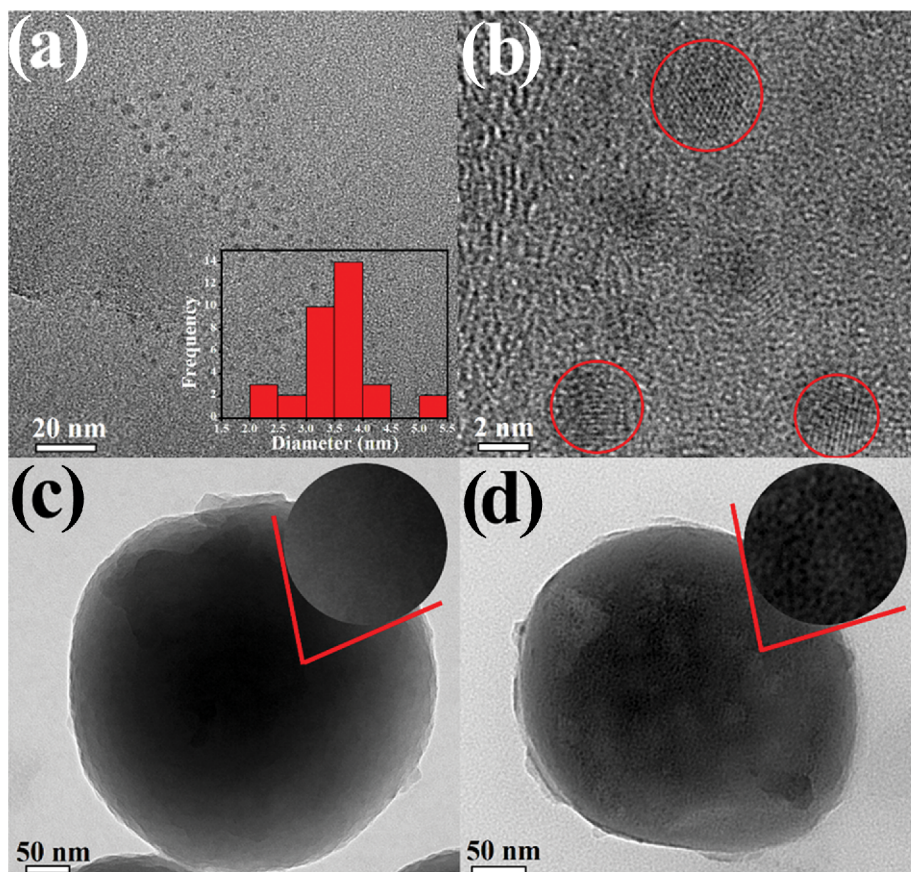


Fig. 2. Excitation (a1), (a2) and emission (b1), (b2) fluorescence spectra of the GQDs and PPy/GQDs (inset: Fluorescence photographs of PPy/GQD composite solution.).



**Scheme 1.** Demonstration of the catecholamine neurotransmitter detection system based on the PPy/GQD composites.



**Fig. 3.** (a) TEM image of GQDs (inset: size distribution of GQDs); (b) HRTEM image of GQDs; and (c), (d) TEM images of PPy microsphere and GQDs inside PPy microsphere (inset: enlarged surface of PPy and PPy/GQDs).

GQDs is more than three times greater than that of the GQDs alone, which can be explained by the presence of amine groups on the PPy backbone. Surface passivation results from the interaction of the oxygen-containing groups in the GQDs, such as hydroxyl and carboxylic acid groups with the nitrogen atoms of PPy through hydrogen bonding and acid-base interactions (Scheme 1). The surface passivation of the GQDs results in an enhancement in the fluorescence intensity [16,24-26]. Moreover, the PPy microspheres also accumulate incompletely carbonized citric acid at the periphery of the composites via  $\pi$ - $\pi$  interactions, which plays a part in surface passivation [24,26].

TEM images (Fig. 3) show morphologies of the composites. As shown, the GQDs were uniformly prepared, having an average size of 3.6 nm (Fig. 3(a)). In the high-resolution (HR)TEM image (Fig. 3(b)), the crystal structure of the GQDs is visible. Fig. 3(c) shows the PPy microsphere structure, having a typically smooth surface. The diameters of the PPy microspheres ranged from 436 to 638 nm, having an average diameter of 533 nm. There is a clear difference in the surface of the PPy/GQDs compared to that of the PPy. Fig. 3(d) shows that the GQDs are attached on PPy microsphere surfaces; in other words, the PPy acts as a platform attracting GQDs.

In addition, characteristics of the composites were analyzed by FTIR spectra. Fig. 4 indicates that the spectrum of PPy has a peak at about  $1,408\text{ cm}^{-1}$ , which is characteristic of C-N bond vibration [28]. Concerning the spectrum of the GQDs, the main characteristic peaks were clearly observed, including a broad absorption band at  $3,030\text{-}3,630\text{ cm}^{-1}$ , which results from O-H stretching of the hydroxyl groups, peaks located in  $1,561$  and  $2,984\text{ cm}^{-1}$ , which are due to the C=C bonding of the aromatic rings and -CH<sub>2</sub> vibrations, respectively, and appearance of peaks at  $1,257$  and  $1,375\text{ cm}^{-1}$ , which is caused by stretching vibrations of the C-O bonds in the carboxylic acid groups. The spectrum of the PPy/GQDs contains all peaks belonging to GQDs. The characteristic peak at  $1,408\text{ cm}^{-1}$  of PPy should be visible in the PPy/GQD spectrum. However, owing to the protonation from the carboxylic acid groups of the GQDs, this peak may shift to shorter wavelengths [28], toward the location of the C-O bonding stretching vibration. Therefore, these peaks could be overlapped. Consequently, there are no clear differences between GQDs and PPy/GQDs spectra.

## 2. Principle of Catecholamine Neurotransmitter Detection

According to previous research, the PPy/GQDs fluorescence

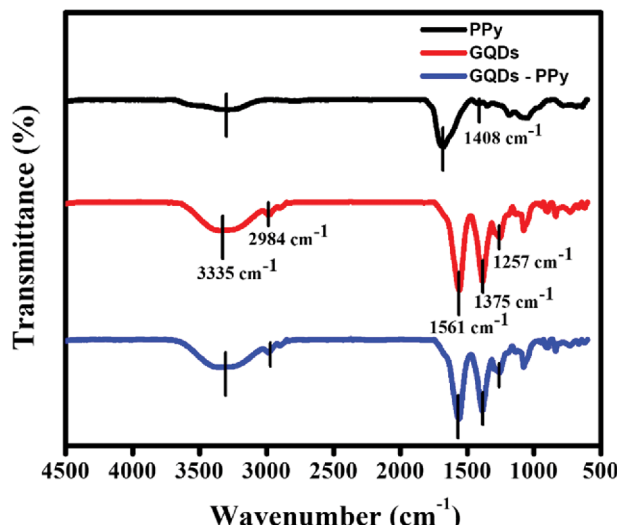
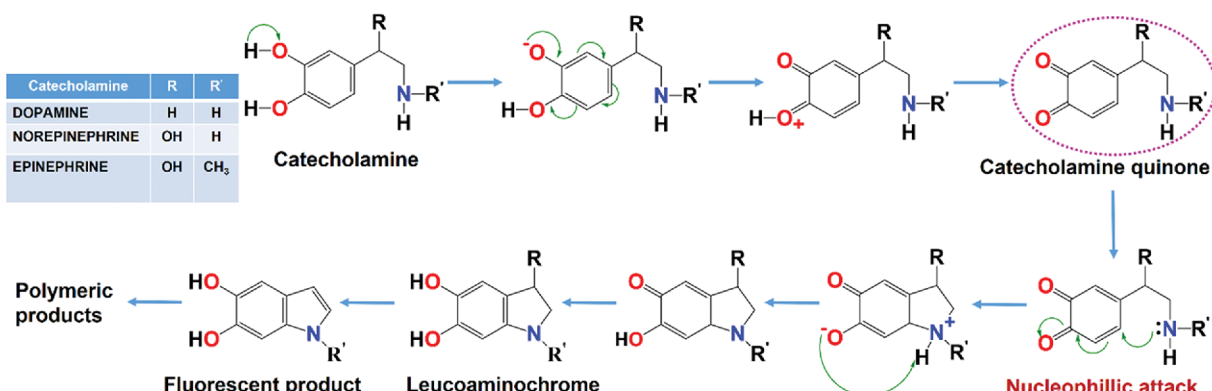


Fig. 4. FTIR spectra of PPy, GQDs, and PPy/GQDs.

intensity gains a highest value and is maintained under pH greater than 7 [26]. When the pH of a solution is adjusted from neutral to alkaline, the catecholamine on the PPy/GQD surface converts to a catecholamine-quinone structure. Under alkaline conditions, the catecholamine-quinone may continue to cyclize via nucleophilic attack, forming a leucoaminochrome and then transforming to a fluorescent product [3,29-32]. In neutral solutions containing GQDs, nucleophilic attack cannot occur; thus, the oxidation of the catecholamine stops at the formation of the catecholamine-quinone structure, which is absorbed onto the PPy/GQDs surface through non-covalent interactions, including hydrogen bonding and electrostatic interaction, and later triggers the fluorescence quenching of the PPy/GQDs [33-36]. The pathway describing the oxidation process of catecholamine is shown in Scheme 2.

There are many molecular interactions, as well as energy and electron transfers, that result in the fluorescence quenching of QDs. From Fig. 5, it can be inferred that fluorescence resonance energy transfer (FRET) is not the mechanism causing the PPy/GQD fluorescence quenching because of no overlapping between the absorption spectrum of the CNs and the emission spectrum of the PPy/GQDs. We determined the zeta potentials values of the PPy/GQDs



Scheme 2. Alkali oxidation of catecholamine.

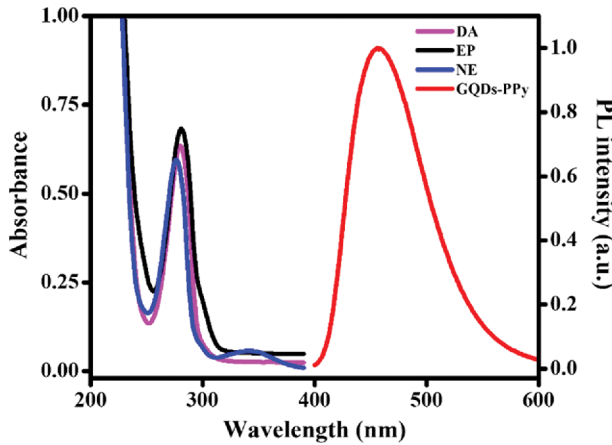


**Fig. 5.** UV-vis spectra of DA, EP, NE and the PL spectrum of the PPy/GQDs.

before and after adding CNs. In the appearance of DA, EP and NE at the same concentration ( $250 \mu\text{M}$ ), the zeta potential of the free PPy/GQDs decreased from  $-35.85 \text{ mV}$  to  $-15.29$ ,  $-25.14$ , and  $-31.83 \text{ mV}$ , respectively (Fig. 6). Thus, there are strong electron transfers between the PPy/GQDs and CNs. In particular, the photo-excited electrons in the conduction band go through intersystem crossing to the  $T_1$  first excited state of GQDs, then transfer to the lowest unoccupied molecular orbital of the catecholamine quinone

leading to the fluorescence quenching of the PPy/GQDs (illustration in Fig. 6) [37]. Catecholamine quinone acts as a good electron acceptor and is kept at a short distance from the donor (QDs) [36,37]. This explains why electrons are held instead of recombining in the  $A_1$  ground state of QDs' therefore, an electron transfer is favored than a recombination process at the interface of the QDs [38-40]. Based on the change in zeta potential, the electron transfer speed from PPy/GQDs to DA-quinone is the fastest, followed by those of EP and NE, respectively.

### 3. Detection of Catecholamine Neurotransmitters

As shown in Fig. 7, in the presence of catecholamine neurotransmitters at a concentration of  $250 \mu\text{M}$ , the fluorescence of the PPy/GQD composites decreased gradually. In particular, after 180 min, DA, EP, and NE quenched 89%, 51%, and 32%, respectively, of the PPy/GQD composite fluorescence intensity. Therefore, the quenching effect of DA on the PPy/GQDs is much more effective and faster than those of EP and NE. The quenching effect is matched to the electron transfer between the PPy/GQDs and CN-quinone structures. Unlike DA, EP and NE contain repulsive groups, including hydroxyl and methyl groups. The presence of these groups results in neighboring group participation [41,42], which could affect the formation of the quinone structure. Therefore, the electron transfer between the PPy/GQDs and quinone structure, which causes the quenching effect, could be affected.

The fluorescence quenching effect of the CNs on the fluorescence intensity of the PPy/GQDs can be seen more clearly in Fig.

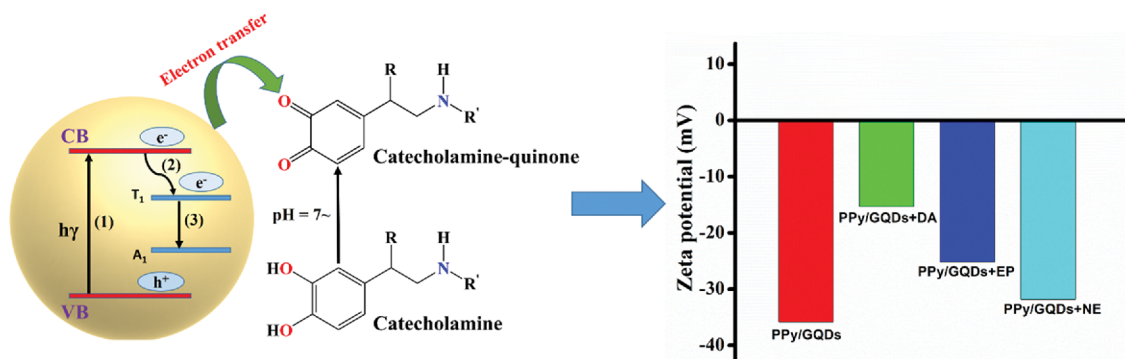


**Fig. 6.** Schematic of the electron transfer process between the PPy/GQD composites and catecholamine-quinone structure, and the zeta potentials of PPy/GQDs and PPy/GQDs+CN ( $250 \mu\text{M}$ ) in PBS.

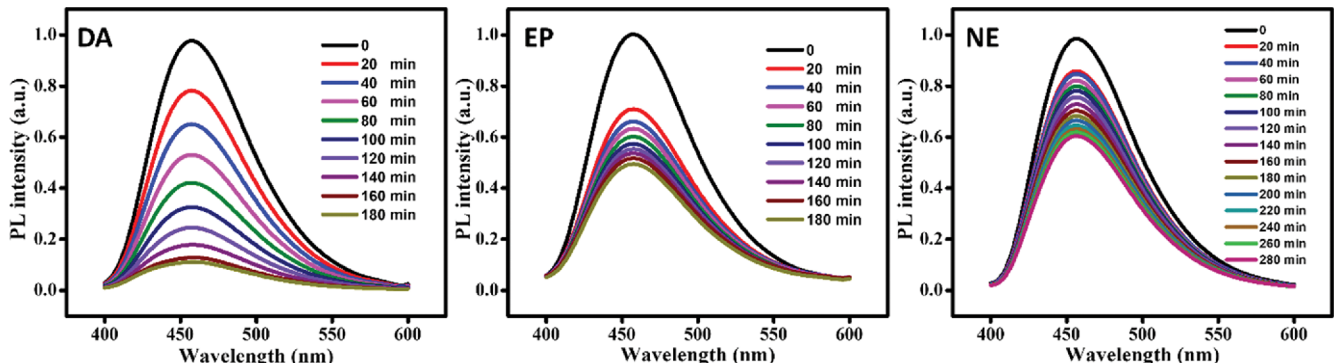


**Fig. 7.** Time response of PPy/GQD fluorescence signals in the presence of DA, EP, and NE at concentration of  $250 \mu\text{M}$ .

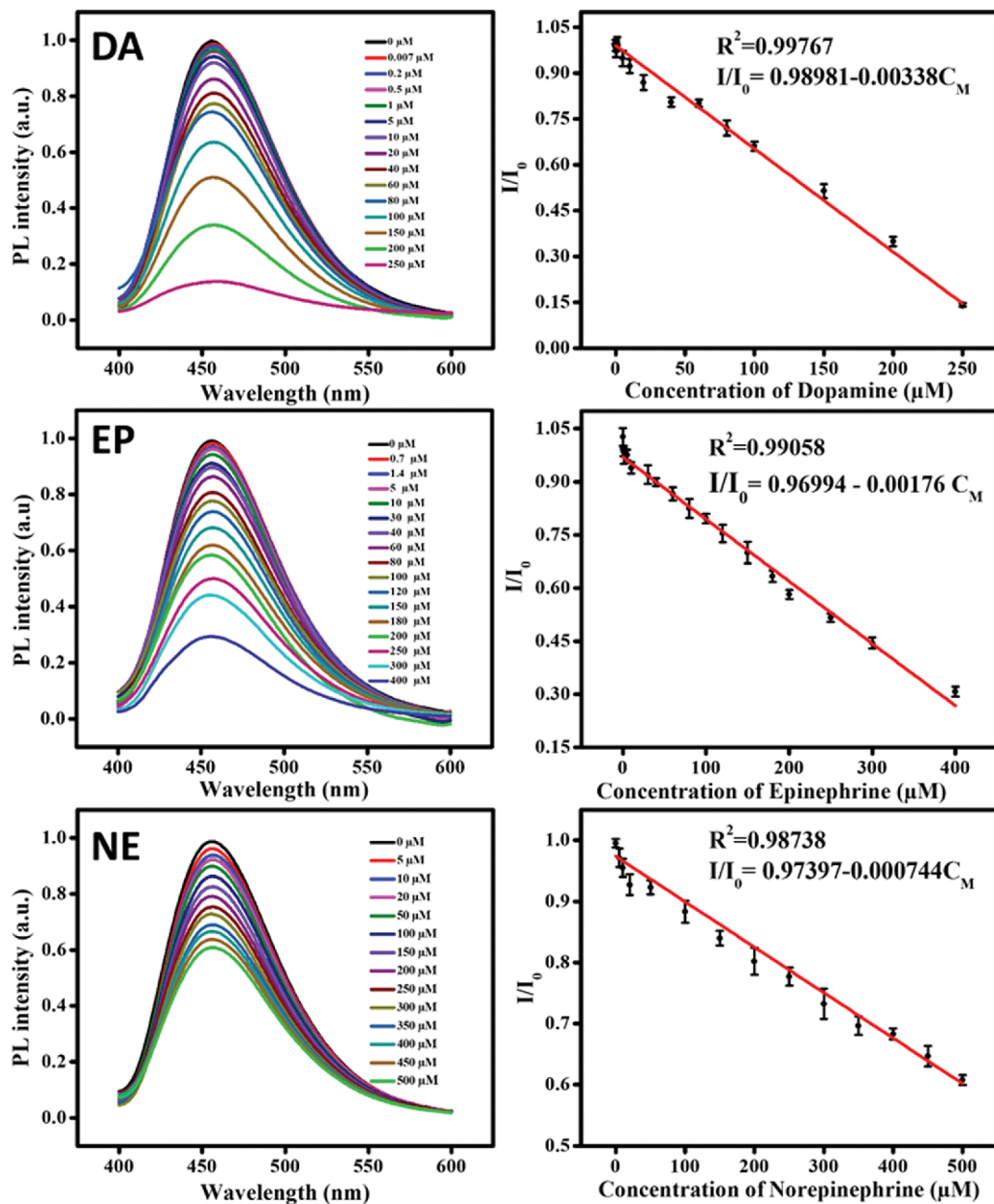


**Fig. 8.** The effect of CN concentration on the fluorescence intensity of PPy/GQD composites and the linear relationship between  $I/I_0$  and the CN concentration.

8. There is a steady decline in the PPy/GQD fluorescence intensity in the presence of the CNs. In addition, Fig. 8 shows the good linear relationships between the relative fluorescence intensity ( $I/I_0$ ,  $I$  and  $I_0$  are the fluorescence emission intensities of the PPy/GQD system in the presence and absence of CNs, respectively) and the concentration of CNs. The minimum concentration of CNs and the linear range at which the analysis can be reliably detected are shown in Table 1. The experiment was repeated three times and data was expressed as the near $\pm$ standard deviation.

#### 4. Detection of Catecholamine Neurotransmitters in Human Serum

To study the practicality and reliability of the PPy/GQD sensor further, we used this system for CN detection in human serum.

**Table 1.** Analytical parameters of the calibration lines

CN	Linear range ( $\mu\text{M}$ )	Limit of detection ( $\mu\text{M}$ )
DA	0-250	0.007
EP	0-400	0.7
NE	0-500	5

Table 2 clearly displays the result. The recovery ranges of DA, EP and NE were 92.1-100.9%, 97.87-106.75%, and 96.67-100.95%, respectively. The experiment was repeated three times and all relative standard deviations (RSDs) were less than 3%, which is acceptable. These results indicate that this method has potential applications for practical detection of CNs such as DA, EP, and NE.

**Table 2. Determination of CNs in human serum**

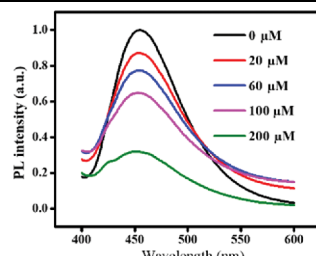
DA				
Samples	Added ( $\mu\text{M}$ )	Found ( $\mu\text{M}$ )	Recovery (%)	RSD (% n=3)
1	20	20.17	100.84	0.57
2	60	59.76	99.60	0.35
3	100	100.90	100.90	0.76
4	200	184.20	92.10	2.99

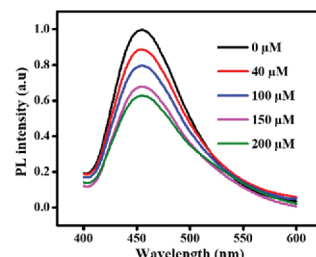
EP				
Samples	Added ( $\mu\text{M}$ )	Found ( $\mu\text{M}$ )	Recovery (%)	RSD (% n=3)
1	40	39.15	97.87	0.38
2	100	100.94	100.94	0.82
3	150	147.06	98.04	0.72
4	200	213.49	106.75	0.55

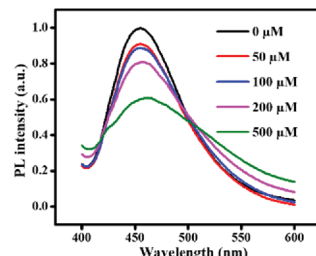
NE				
Samples	Added ( $\mu\text{M}$ )	Found ( $\mu\text{M}$ )	Recovery (%)	RSD (% n=3)
1	50	49.80	99.58	0.105
2	100	100.95	100.95	0.257
3	200	200.37	100.18	0.506
4	500	483.34	96.67	0.321



The effect of DA concentration on the fluorescence intensity of PPy/GQD composites in human serum



The effect of EP concentration on the fluorescence intensity of PPy/GQD composites in human serum



The effect of NE concentration on the fluorescence intensity of PPy/GQD composites in human serum

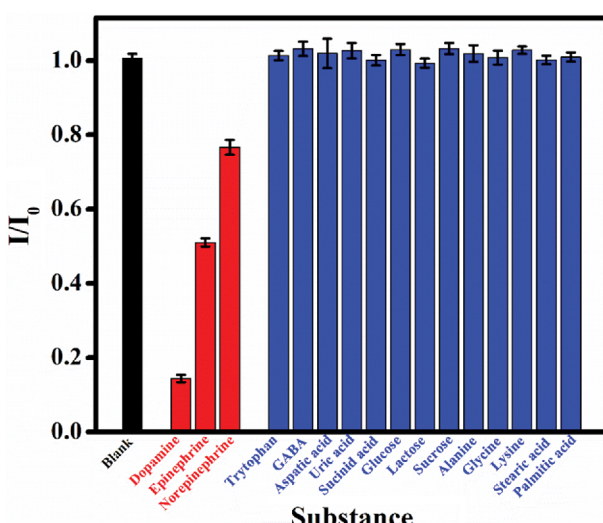
## 5. Selectivity Study

Sensors not only require sensitivity but also high specificity, which is particularly necessary in detecting a real sample. To confirm that the presented method is specific for CN sensing, the fluores-

cent responses in the presence of carbohydrates, amino acids, and other common molecules were studied and compared with those of CNs at the same concentration. Fig. 9 shows that the selective quenching effect of the CNs is significantly greater than other substances, which shows that the PPy/GQD system exhibited excellent selectivity for CN detection.

## CONCLUSION

We successfully synthesized a PPy/GQD composite material with excellent fluorescence properties compared to those of traditional GQDs. Furthermore, we designed a simple and convenient sensor based on this material for CN detection. The sensor is highly sensitive, selective, and effective. Our method applies on fluorescence quenching effect via a photo-induced electron transfer process. Among the three catecholamine neurotransmitters studied, the quenching effect of dopamine was much faster and more effective than that of epinephrine and norepinephrine. In comparison to the reported methods for CN detection, our sensor is simply designed, easily operated and does not demand expensive equipment or complicated procedures. Moreover, this strategy may be successfully used for the detection of CNs in real samples. As a result, we believe that this technique will open a new direction for development of easy-operating, rapid, sensitive and inexpensive sensors

**Fig. 9. Effect of 250  $\mu\text{M}$  of physiological molecules on the fluorescence intensity of the PPy/GQD.**

for the detection of CNs as well as potential biomedical and environmental applications.

### ACKNOWLEDGEMENT

This research was supported by Basic Science Research Capacity Enhancement Project through Korea Basic Science Institute (National research Facilities and Equipment Center) grant funded by the Ministry of Education (Grant No. 2019R1A6C1010016) and the Gachon University research fund of 2019 (GCU-2019-0322).

### REFERENCES

- T. Pradhan, H. S. Jung, J. H. Jang, T. W. Kim, C. Kang and J. S. Kim, *Chem. Soc. Rev.*, **43**(13), 4684 (2014).
- J. A. Ribeiro, P. M. V. Fernandes, C. M. Pereira and F. Silva, *Talanta*, **160**, 653 (2016).
- F. Ghasemi, M. R. Hormozi-Nezhad and M. Mahmoudi, *Anal. Chim. Acta*, **917**, 85 (2016).
- B. Mekassa, M. Tessema, B. S. Chandravanshi, P. G. L. Baker and F. N. Muya, *J. Electroanal. Chem.*, **807**, 145 (2017).
- S. A. Zaidi, *Electrochim. Acta*, **274**, 370 (2018).
- A. Azzouz, K. Y. Goud, N. Raza, E. Ballesteros, S. E. Lee, J. Hong, A. Deep and K. H. Kim, *Trac-Trends Anal. Chem.*, **110**, 15 (2019).
- A. Azaryan, T. Ligor, B. Buszewski, A. Temerdashev, E. Dmitrieva and E. Gashimova, *Chromatographia*, **81**(11), 1487 (2018).
- Z. P. Liu, M. L. Jin, J. P. Cao, R. W. Niu, P. F. Li, G. F. Zhou, Y. Yu, A. van den Berg and L. L. Shui, *Sens. Actuator B-Chem.*, **273**, 873 (2018).
- T. H. Le, J. H. Kim and S. J. Park, *J. Crystal Growth*, **468**, 788 (2017).
- Y. M. Liu, Z. L. Liu and Y. M. Shi, *Luminescence*, **26**(1), 59 (2011).
- J. Y. Huang, W. T. Xu, Y. Q. Gong, S. H. Weng and X. H. Lin, *Int. J. Electrochem. Sci.*, **11**(10), 8193 (2016).
- Z. Y. Zhu, C. Ravelet, S. Perrier, V. Guieu, B. Roy, C. Perigaud and E. Peyrin, *Anal. Chem.*, **82**(11), 4613 (2010).
- K. C. Ko, J. S. Wu, H. J. Kim, P. S. Kwon, J. W. Kim, R. A. Bartsch, J. Y. Lee and J. S. Kim, *Chem. Commun.*, **47**(11), 3165 (2011).
- J. S. Kim, H. J. Kim, H. M. Kim, S. H. Kim, J. W. Lee, S. K. Kim and B. R. Cho, *J. Org. Chem.*, **71**(21), 8016 (2006).
- S. Campuzano, P. Yanez-Sedeno and J. M. Pingarron, *Nanomaterials*, **9**(4), 18 (2019).
- X. T. Liu, W. D. Na, H. Liu and X. G. Sue, *Biosens. Bioelectron*, **98**, 222 (2017).
- L. X. Lin and S. W. Zhang, *Chem. Commun.*, **48**(82), 10177 (2012).
- X. Q. Yu, W. S. Zhang, P. P. Zhang and Z. Q. Su, *Biosens. Bioelectron*, **89**, 72 (2017).
- H. D. Pham, V. H. Pham, E. S. Oh, J. S. Chung and S. Kim, *Korean J. Chem. Eng.*, **29**(1), 125 (2012).
- S. S. Jeon, C. Kim, J. Ko and S. S. Im, *J. Mater. Chem.*, **21**(22), 8146 (2011).
- R. Sun, H. Y. Chen, Q. W. Li, Q. J. Song and X. T. Zhang, *Nanoscale*, **6**(21), 12912 (2014).
- S. Chatterjee, A. Shit and A. K. Nandi, *J. Mater. Chem. A*, **1**(39), 12302 (2013).
- C. Yang, C. X. Xu and X. M. Wang, *Langmuir*, **28**(9), 4580 (2012).
- Y. Q. Dong, G. L. Li, N. N. Zhou, R. X. Wang, Y. W. Chi and G. N. Chen, *Anal. Chem.*, **84**(19), 8378 (2012).
- J. H. Shen, Y. H. Zhu, X. L. Yang and C. Z. Li, *Chem. Commun.*, **48**(31), 3686 (2012).
- X. Zhou, P. P. Ma, A. Q. Wang, C. F. Yu, T. Qian, S. S. Wu and J. Shen, *Biosens. Bioelectron.*, **64**, 404 (2015).
- L. P. Lin, M. C. Rong, F. Luo, D. M. Chen, Y. R. Wang and X. Chen, *Trac-Trends Anal. Chem.*, **54**, 83 (2014).
- P. Routh, S. Das, A. Shit, P. Bairi, P. Das and A. K. Nandi, *ACS Appl. Mater. Interfaces*, **5**(23), 12672 (2013).
- S. Hong, Y. S. Na, S. Choi, I. T. Song, W. Y. Kim and H. Lee, *Adv. Funct. Mater.*, **22**(22), 4711 (2012).
- J. H. Lin, C. J. Yu, Y. C. Yang and W. L. Tseng, *Phys. Chem. Chem. Phys.*, **17**(23), 15124 (2015).
- A. Yildirim and M. Bayindir, *Anal. Chem.*, **86**(11), 5508 (2014).
- J. M. Zen, A. S. Kumar and J. C. Chen, *Electroanalysis*, **13**(6), 457 (2001).
- R. Gill, R. Freeman, J. P. Xu, I. Willner, S. Winograd, I. Shweky and U. Banin, *J. Am. Chem. Soc.*, **128**(48), 15376 (2006).
- Z. Z. Li, Q. Y. Zhang, H. Y. Huang, C. J. Ren, S. Ouyang and Q. Zhao, *Talanta*, **171**, 16 (2017).
- S. Y. Liu, F. P. Shi, L. Chen and X. G. Su, *Sens. Actuator B-Chem.*, **191**, 246 (2014).
- I. L. Medintz, M. H. Stewart, S. A. Trammell, K. Susumu, J. B. Delehaney, B. C. Mei, J. S. Melinger, J. B. Blanco-Canosa, P. E. Dawson and H. Mattossi, *Nat. Mater.*, **9**(8), 676 (2010).
- D. Diaz-Diestra, B. Thapa, J. Beltran-Huarac, B. R. Weiner and G. Morell, *Biosens. Bioelectron.*, **87**, 693 (2017).
- R. Ban, E. S. Abdel-Halim, J. R. Zhang and J. J. Zhu, *Analyst*, **140**(4), 1046 (2015).
- Q. Mu, H. Xu, Y. Li, S. J. Ma and X. H. Zhong, *Analyst*, **139**(1), 93 (2014).
- X. D. Zhang, X. K. Chen, S. Q. Kai, H. Y. Wang, J. J. Yang, F. G. Wu and Z. Chen, *Anal. Chem.*, **87**(6), 3360 (2015).
- R. Kudoh, A. Sudo and T. Endo, *Macromolecules*, **43**(3), 1185 (2010).
- Y. P. Wang, T. Cheng, J. L. Sun, Z. C. Liu, M. Frasconi, W. A. Goddard and J. F. Stoddart, *J. Am. Chem. Soc.*, **140**(42), 13827 (2018).